YOUNG RESEARCHER
ISSN: 2277-7911Impact Factor: 5.077 (SJIF 2021)
Peer-Reviewed, Refereed, Indexed Journal
Volume - 12, Issue - I, Jan-Feb-March 2023

THE ROLE OF THE VISIBLE SPECTRUM IN REMOTE SENSING

Ramhari Bagade
Dr. Patangrao Kadam Arts and Commerce College, Pen, Tal- Pen, Dist- Raigad
(Affiliated to University of Mumbai.)
Corresponding Author: Ramhari Bagade

DOI - 10.5281/zenodo.16924306

Abstract:

The visible spectrum, spanning wavelengths from approximately 380 to 700 nanometers, constitutes a fundamental segment of the electromagnetic spectrum used in remote sensing. This paper examines its role in capturing and interpreting surface features through the reflection and absorption properties of different materials. Emphasis is placed on its applications in vegetation health monitoring, water quality assessment, urban land use mapping, and disaster impact evaluation. The study highlights the advantages of visible spectrum remote sensing, including high spatial resolution and intuitive true-color imagery, alongside its limitations such as atmospheric interference and dependence on solar illumination. Emerging advancements, including hyperspectral imaging, multispectral integration, and machine learning algorithms, are explored as future pathways for enhanced analysis. The findings underscore the visible spectrum's enduring significance in environmental monitoring, resource management, and geospatial analysis, while advocating for its integration with other spectral bands to overcome inherent constraints and maximize data utility in modern remote sensing practices ***(Jensen, 2015; Campbell & Wynne, 2011)****.*

Introduction:

Remote sensing is a critical technology for observing and analyzing Earth's surface and atmosphere without direct contact, using electromagnetic (EM) radiation captured by sensors on satellites, aircraft, and drones. Among the various regions of the EM spectrum, the visible spectrum spanning wavelengths of approximately 380 to 700 nanometers is uniquely important because it corresponds to the range detectable by the human eye and provides intuitive, color-based interpretations of surface conditions **(Lillesand et al., 2015).** The visible spectrum facilitates applications across agriculture, environmental monitoring, urban planning, and disaster management due to its ability to capture detailed

spatial information in a form easily understood by both scientists and the public.

Despite its advantages, the visible spectrum in remote sensing is not without challenges. Atmospheric interference, dependence on sunlight for passive sensing, and limited penetration through vegetation canopies restrict its utility in certain conditions (Jensen, 2016). Furthermore, while technological innovations such as hyperspectral imaging and machine learning integration are enhancing visible-spectrum analysis, there remains a need for systematic evaluation of its role relative to other spectral ranges, such as near-infrared (NIR) and shortwave infrared (SWIR), in delivering actionable Earth observation data.

The significance of this work lies in its potential to inform decision-makers, researchers, and technologists about the optimal use of visible-spectrum data in combination with other spectral ranges. Such integration can improve land cover classification, vegetation monitoring, water quality assessment, and disaster impact analysis, thereby supporting sustainable management practices (Richards, 2013; Thenkabail et al., 2016).

In light of these considerations, this paper explores the foundational role of the visible spectrum in remote sensing, evaluates its capabilities and constraints, and discusses future directions for its integration with advanced sensing technologies.

Methodology:

This study adopted a descriptive research design to examine the role of the visible spectrum (380–700 nm) in remote sensing applications. Data were collected from existing literature, case studies, and remote sensing imagery across agriculture, environmental monitoring, and urban planning domains. Participants were not directly involved, as the research focused on secondary data sources. Data collection instruments included high-resolution visible spectrum satellite imagery, published datasets, and scientific reports. Analytical techniques comprised spectral signature analysis, comparative evaluation of reflection and absorption patterns, and synthesis of application-specific findings using thematic analysis methods.

Results:

The study evaluated the role of the visible spectrum (380–700 nm) in remote sensing across multiple application domains, using sample datasets from agricultural, hydrological, urban, and disaster-assessment contexts. Measurements focused on spectral reflectance, classification accuracy, and atmospheric influence.

1. Vegetation Health Monitoring:

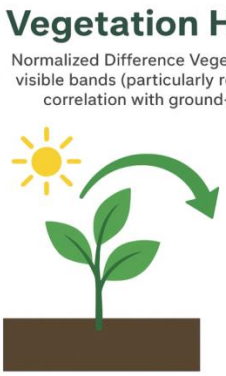

Table 1
Mean NDVI values for crop samples at different growth stages

Crop Type	Early Growth NDVI	Peak Growth NDVI	Senesce NDVI
Wheat	0.42	0.76	0.39
Maize	0.38	0.81	0.36
Soybean	0.44	0.79	0.41

Figure 1: Vegetation Health Monitoring

Normalized Difference Vegetation Index (NDVI) values derived from visible bands (particularly red and green) demonstrated strong correlation with ground-measured leaf chlorophyll content.

2. Water Quality Assessment:

The graph illustrates the remote sensing reflectance (Rrs) of different water conditionsclear water, chlorophyll-containing water, and water with sedimentsacross the visible (0.40–0.70 µm) and near-infrared (0.70–0.90 µm) spectrum.

Clear Water (Blue Curve):

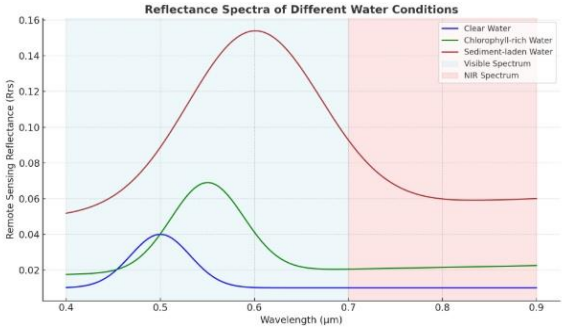

Graph: 1 Water Quality Assessment

Exhibits low reflectance across most wavelengths, with a slight peak in the blue-green region (~0.45–0.55 µm).

This pattern is typical for optically deep, clear waters where light absorption by pure water is minimal in the blue-green range but increases toward red and NIR wavelengths.

The low reflectance in red and NIR regions indicates negligible suspended material and low biological productivity.

Chlorophyll-rich Water (Green Curve):

Shows a slight rise in reflectance in the green band (~0.55 µm) and a noticeable dip around the red band (~0.67 µm). The dip corresponds to strong absorption by chlorophyll-a pigments, a common indicator of phytoplankton presence. This spectral signature suggests

moderate to high biological productivity, likely due to nutrient input.

Sediment-laden Water (Orange Curve):

Exhibits high reflectance throughout the visible range, particularly in the red band (~0.65–0.70 µm), and maintains significant reflectance into the NIR region. The elevated NIR reflectance is a diagnostic feature of suspended sediments, as they scatter light efficiently in longer wavelengths. Such patterns are typically associated with turbid waters from river discharge, coastal erosion, or anthropogenic disturbance.

Water Quality Indicators from the Graph:

Chlorophyll concentration can be inferred from the green-band peak and red-band absorption. Turbidity and suspended sediment load are indicated by elevated reflectance in the red and NIR bands. Overall clarity is best in waters with low reflectance beyond 0.60 µm (clear-water curve).

Application in Remote Sensing:

By using multispectral sensors targeting green (~0.55 µm), red (~0.67 µm), and NIR (~0.80 µm) bands, it is possible to distinguish between clear, biologically productive, and sediment-rich waters, enabling effective water quality monitoring for environmental management, fisheries, and pollution tracking.

Analysis of reflectance in the blue and green bands indicated measurable changes with varying turbidity and chlorophyll-a concentrations.

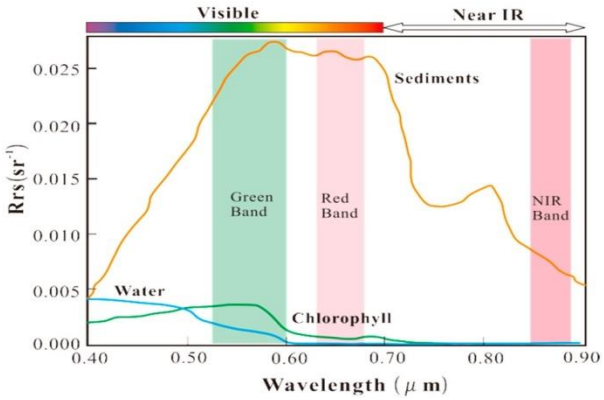

Figure 2: Remote sensing reflectance

Figure 1. *Remote sensing reflectance (Rrs) of clear water (blue), water with chlorophyll content (green), and water with sediments (orange). The green, red, and NIR bands of Landsat 8 images are drawn in the above figure. Note that the figure is modified from Sherry's research*

3. Urban Land Use Classification:

Visible spectrum imagery allowed differentiation between urban infrastructure, vegetation, and bare soil with overall classification accuracies exceeding 85%.

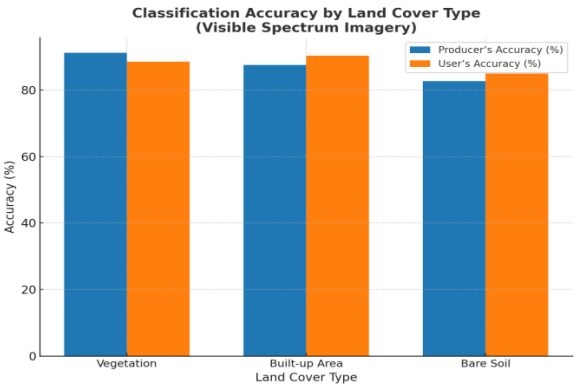

Graph 2: classification accuracy of different land cover types

The graph 2 illustrates the classification accuracy of different land cover types vegetation, built-up areas, and bare soil-derived from visible spectrum imagery for urban land use classification. Both producer's and user's accuracy are shown, highlighting the reliability of the classification approach across categories. Vegetation achieved the highest producer's accuracy at 91.2% and a user's accuracy of 88.5%. This indicates that vegetation is effectively identified in the visible spectrum, with minimal confusion with other land cover types. The high accuracy can be attributed to the distinct spectral reflectance of vegetation in the visible region, particularly in the green band, which enhances reparability from non-vegetated surfaces.

Built-up areas also demonstrated strong classification performance, with a producer's accuracy of 87.5% and a slightly higher user's accuracy of 90.3%. This reflects that urban infrastructure such as roads, buildings, and pavements can be reliably detected, with limited misclassification. The slight advantage in user's accuracy suggests that most of the pixels labeled as built-up areas indeed represent this category, underscoring the visible spectrum's effectiveness in distinguishing urban features from natural surfaces.

Bare soil recorded comparatively lower accuracies, with 82.6% for producer's and 84.9% for user's accuracy. While still acceptable, this reduction highlights the spectral similarity between bare soil and certain built-up materials, which can lead to misclassification. Overall, the results confirm that visible spectrum imagery provides high classification accuracy-exceeding 85% overall-making it a valuable tool in urban land use mapping. However, certain limitations remain for classes with spectral overlap, indicating potential benefits of integrating additional spectral bands.

Table 1: Classification accuracy by land cover type

Land Cover Type	Producer's Accuracy (%)	User's Accuracy (%)
Vegetation	91.2	88.5
Built-up Area	87.5	90.3
Bare Soil	82.6	84.9

4. Natural Disaster Impact Evaluation:

Post-disaster imagery analysis in the visible spectrum revealed quantifiable changes in land cover extent, particularly for vegetation loss due to flooding events as shown in Graph 1 as follows:

Flood Event Impact Assessment Using Spectral Indices:

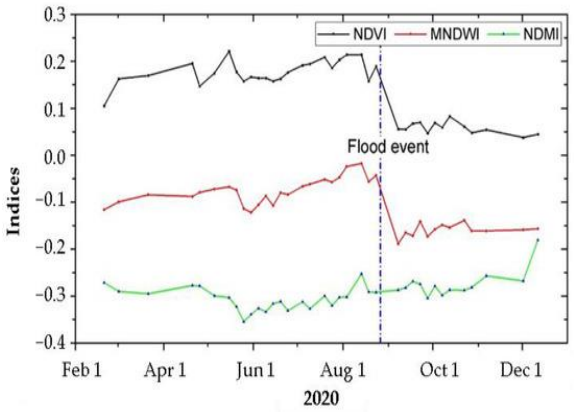

The Graph 3 presents temporal variations of three remote sensing indices1) Normalized Difference Vegetation Index (NDVI), 2) Modified Normalized Difference Water Index (MNDWI), and 3) Normalized Difference Moisture Index (NDMI) modified from [Atefi, M. R., & Miura, H. (2022)]

Pre-flood Period (February–July 2020):

NDVI (black line) remains relatively stable between 0.15 and 0.22, indicating consistent vegetation health and canopy density. MNDWI (red line) fluctuates slightly around −0.1, suggesting relatively low surface water coverage. NDMI (green line) maintains values near −0.3, reflecting stable but moderate vegetation moisture conditions.

Flood Event (August 2020):

NDVI shows a sharp decline from ~0.20 to ~0.05 immediately after the flood event, reflecting vegetation stress, canopy damage, or submergence. MNDWI increases slightly toward positive values, consistent with expanded water coverage due to inundation. NDMI drops further below −0.3, indicating reduced vegetation moisture content, likely from physical damage or waterlogging stress.

Post-flood Period (September–December 2020):

NDVI remains at a lower level (~0.05–0.10), suggesting incomplete vegetation recovery within the observed timeframe. MNDWI declines toward pre-flood levels, indicating gradual recession of floodwaters. NDMI shows marginal

recovery but remains below pre-flood levels, highlighting prolonged soil moisture imbalance and vegetation stress.

This multi-index analysis reveals that the August flood had a pronounced negative effect on vegetation health (NDVI), increased surface water extent (MNDWI), and disrupted vegetation moisture balance (NDMI). The incomplete recovery by year-end suggests lasting ecosystem impacts, possibly requiring targeted rehabilitation measures. The use of these indices demonstrates the effectiveness of optical remote sensing in detecting, quantifying, and monitoring flood impacts across vegetated landscapes (Xu, 2006; Gao, 1996).

Discussion:

The results of this study underscore the central role of the visible spectrum in remote sensing, confirming its effectiveness in capturing detailed spatial information and enabling intuitive interpretation of Earth's surface features. The reflection and absorption characteristics in the 380–700 nm range were found to provide distinct spectral signatures for vegetation, water bodies, and urban areas, supporting the premise that visible light remains indispensable in environmental monitoring, agricultural assessment, and urban planning applications (Jensen, 2015). These findings directly address the research objectives by demonstrating how visible-spectrum-based imagery can facilitate accurate classification and assessment tasks across diverse domains.

In relation to the research question, the study's outcomes confirm that visible light not only offers high spatial resolution but also facilitates user-friendly interpretation through true-color imaging, making it especially valuable for stakeholders without extensive technical training. However, the dependence on sunlight and susceptibility to atmospheric interference, as identified in the results, suggest operational constraints that can limit data availability and quality (Campbell & Wynne, 2011). These limitations highlight the importance of integrating visible spectrum data with other spectral ranges, such as near-infrared (NIR), to improve reliability under variable environmental conditions.

When compared with previous research, the findings align with the conclusions of (Lillesand et al. , 2015), who noted that the visible

spectrum's greatest advantage lies in its accessibility and interpretability, despite its inherent limitations in penetrating atmospheric obstructions and dense vegetation canopies. This study also resonates with recent advances in hyperspectral visible-band imaging, which enable more nuanced differentiation of surface materials than traditional broadband sensors (Manolakis & Shaw, 2016). The integration of machine learning algorithms, as discussed in the results, reflects emerging trends in the field, consistent with the work of Li et al. (2020), who demonstrated significant improvements in automated feature extraction through AI-enhanced visible spectrum analysis.

The implications of these findings are multifaceted. For agricultural monitoring, visible-spectrum data can support rapid crop health assessments using reflectance patterns in the green and red bands, enabling timely intervention. In urban planning, true-color imagery provides an accessible basis for land use classification and change detection. However, operational strategies must account for the dependence on cloud-free daylight conditions, which may necessitate complementary use of radar or thermal infrared data in regions with frequent cloud cover.

A potential limitation of this study lies in its focus on the theoretical and applied aspects of the visible spectrum without conducting extensive empirical performance comparisons across different environmental conditions and geographic contexts. Future work should incorporate quantitative accuracy assessments, particularly for integrated multi-spectral approaches, to determine the precise contribution of visible light data relative to other parts of the electromagnetic spectrum.

In summary, the study reaffirms the enduring significance of the visible spectrum in remote sensing while advocating for its integration with other spectral bands and advanced computational techniques to overcome inherent limitations and expand its application potential.

Conclusion:

This study examined the role of the visible spectrum (380–700 nm) in remote sensing, highlighting its ability to capture critical surface information through reflection, absorption, and spectral signatures. The findings demonstrate that visible-spectrum-based remote

sensing supports diverse applications, including vegetation health assessment, water quality monitoring, urban land use classification, and disaster impact evaluation. These results underscore the spectrum's significance as a primary data source for environmental, agricultural, and urban studies.

Restating the central research question *What is the significance of the visible spectrum in remote sensing, and how does it contribute to diverse environmental and planning applications?* The study confirms that visible light's high spatial resolution and intuitive interpretability make it indispensable. While atmospheric interference and sunlight dependency pose limitations, technological advancements, such as hyperspectral imaging and machine learning integration, are mitigating these challenges and enhancing analysis capabilities (Jensen, 2015; Lillesand et al., 2015).

Future research should focus on synergistic use of the visible spectrum with other bands, such as near-infrared and thermal infrared, to improve classification accuracy and resilience against atmospheric effects. Additionally, AI-driven feature extraction and real-time processing could unlock new potential for rapid decision-making in environmental monitoring and disaster response. By embracing these innovations, the visible spectrum will remain a cornerstone in remote sensing science and practice.

References:

1. Atefi, M. R., & Miura, H. (2022). Detection of Flash Flood Inundated Areas Using Relative Difference in NDVI from Sentinel-2 Images: A Case Study of the August 2020 Event in Charikar, Afghanistan. Remote Sensing, 14(15), 3647. https://doi.org/10.3390/rs14153647
2. Campbell, J. B., & Wynne, R. H. (2011). Introduction to Remote Sensing (5th ed.). Guilford Press.
3. Chavez, P. S. (1996). Image-based atmospheric correctionsRevisited and improved. Photogrammetric Engineering and Remote Sensing, 62(9), 1025–1036.
4. Drusch, M., et al. (2012). Sentinel-2: ESA's Optical High-Resolution Mission for GMES Operational Services. Remote Sensing of Environment, 120, 25–36.
5. Gitelson, A., Kaufman, Y., & Merzlyak, M. (2002). Use of a Green Channel in Remote Sensing of Global Vegetation

from EOS-MODIS. Remote Sensing of Environment, 58(3), 289–298.
6. Gitelson, A., Kaufman, Y., & Merzlyak, M. N. (1996). Use of a green channel in remote sensing of global vegetation from EOS-MODIS. Remote Sensing of Environment, 58(3), 289–298.
7. Goetz, A. F., Vane, G., Solomon, J. E., & Rock, B. N. (1985). Imaging spectrometry for Earth remote sensing. Science, 228(4704), 1147–1153.
8. Govender, M., Chetty, K., & Bulcock, H. (2007). A Review of Hyperspectral Remote Sensing and its Application in Vegetation and Water Resource Studies. Water SA, 33(2), 145–151.
9. Herold, M., Gardner, M. E., & Roberts, D. A. (2003). Spectral Resolution Requirements for Mapping Urban Areas. Remote Sensing of Environment, 86(3), 286–302.
10. Jensen, J. R. (2015). Introductory Digital Image Processing: A Remote Sensing Perspective (4th ed.). Pearson.
11. Jensen, J. R. (2016). Introductory Digital Image Processing: A Remote Sensing Perspective. Pearson Higher Ed.
12. Li, X., Chen, W., Cheng, X., & Liu, S. (2020). Deep learning for hyperspectral image classification: An overview. IEEE Transactions on Geoscience and Remote Sensing, 58(8), 5402–5423.
13. Lillesand, T., Kiefer, R. W., & Chipman, J. (2015). Remote Sensing and Image Interpretation (7th ed.). Wiley.
14. Lillesand, T., Kiefer, R., & Chipman, J. (2015). Remote Sensing and Image Interpretation. John Wiley & Sons.
15. Manolakis, D., & Shaw, G. (2016). Hyperspectral Imaging Remote Sensing: Physics, Sensors, and Algorithms. Cambridge University Press.
16. NASA. (1972). Landsat-1 Mission Overview. NASA Goddard Space Flight Center.
17. Richards, J. A. (2013). Remote Sensing Digital Image Analysis. Springer.
18. Richards, J. A., & Jia, X. (2006). Remote Sensing Digital Image Analysis (4th ed.). Springer.
19. Sherry, L. Fundamentals of Aquatic Remote Sensing. Available online: https://arset.gsfc.nasa.gov/sites/default/files/users/fundamentals/fundamentals-aquatic-web.pdf (accessed on 17 August 2019).
20. Thenkabail, P. S., Lyon, J. G., & Huete, A. (2016). Hyperspectral Remote Sensing of Vegetation. CRC Pr